Cancer Immunology, Immunotherapy (2026) 75:99
https://doi.org/10.1007/s00262-026-04343-w

RESEARCH

Protein-level profiling of TIGIT axis components in human PDAC reveals immune–suppressive expression patterns

D. Quatannens[1] · Y. Verhoeven[1] · S. van der Heijden[1] · D. Peeters[2] · J. Claes[3] · C. Hermans[1] · H. Lambrechts[1] · K. Zwaenepoel[2] · P. van Dam[1,4] · M. Peeters[1] · H. Prenen[1,4] · S. Koljenovic[1,2] · J. De Waele[1] · C. Faes[3] · F. Lardon[1] · G. Roeyen[5] · E. Smits[1] · J. Van Audenaerde[1]

Received: 14 October 2025 / Accepted: 16 February 2026

Abstract

Purpose In pancreatic ductal adenocarcinoma (PDAC), immune checkpoint inhibitors have shown limited efficacy, and the role of the TIGIT axis remains underexplored. This study aimed to characterize TIGIT axis components on protein level and their relationship to PD-1/PD-L1 expression in matched blood and tumor samples from PDAC patients to identify immunosuppressive mechanisms and fuel future strategies for immune checkpoint co-targeting in PDAC patients.

Experimental design Fresh tumor and peripheral blood samples were collected from PDAC patients undergoing surgical resection. Flow cytometry was performed on tumor-infiltrating lymphocytes and PBMCs to assess expression of TIGIT, DNAM-1, TACTILE, and PD-1. Ligands CD111, CD112, CD113, and CD155 were analyzed using immunohistochemistry. Additional RNA expression analysis (TCGA/GTEx) was used to evaluate ligand distribution and gene expression profiles.

Results TIGIT was highly upregulated on intratumoral $CD8^+$ T cells and regulatory T cells, frequently co-expressed with PD-1. DNAM-1 expression was significantly reduced in tumors. However, contrasting pattern emerges with Tregs, which uniquely upregulate DNAM-1 in the PDAC TME. In addition, CD112 and CD155 were broadly expressed, including novel stromal CD112 localization. NK cells were nearly absent intratumorally, correlating with DNAM-1 downregulation.

Conclusions Our findings identify TIGIT as a promising immunotherapeutic target in PDAC and suggest that dual checkpoint blockade (TIGIT/PD-1), alongside restoration of DNAM-1 signaling, may overcome immune suppression. These results provide mechanistic rationale to inform future clinical trials in PDAC.

Keywords Immune checkpoints · Pancreatic cancer · TIGIT axis · Tumor immune microenvironment

Introduction

Pancreatic ductal adenocarcinoma (PDAC) remains one of the most lethal cancer types and is predicted to become the second leading cause of cancer-related deaths by 2030 [1]. The 5-year overall survival rate remains below 10%, with little improvement over the past decades. This is due to the prevalence of therapy resistance, which continues to be a major obstacle in clinical treatment [2]. Surgical resection of the tumor remains the only curative option for PDAC patients. However, only a 20% of the patients are eligible for surgery, as most patients are diagnosed at late-stage, with locally advanced or metastatic disease [3–6]. Therefore, systemic chemotherapy is the mainstay treatment for most PDAC patients, with the standard of care being FOLFIRINOX for those with a high-performance status and gemcitabine plus nab-paclitaxel for others [7].

E. Smits and J. Van Audenaerde have contributed equally to this work.

✉ J. Van Audenaerde
jonas.vanaudenaerde@uantwerpen.be

1 Center for Oncological Research (CORE), Integrated Personalized and Precision Oncology Network (IPPON), University of Antwerp, Antwerp, Belgium

2 Department of Pathology, Antwerp University Hospital (UZA), Antwerp, Belgium

3 Data Science Institute, I-Biostat, Hasselt University, Hasselt, Belgium

4 Department of Oncology, Antwerp University Hospital (UZA), Antwerp, Belgium

5 Department of Hepatobiliary Transplantation and Endocrine Surgery, Antwerp University Hospital (UZA), Antwerp, Belgium

Published online: 10 March 2026

The emergence of immune checkpoint inhibitors (ICI), targeting the programmed cell death protein-1/programmed death ligand-1 (PD-1/PD-L1) axis and cytotoxic T-lymphocyte–associated protein 4 (CTLA-4), has revolutionized cancer treatment for several cancer types [8]. However, early clinical studies evaluating these ICI, both as monotherapies and in combination, failed to demonstrate objective responses in PDAC patients [9–12]. This limited efficacy of ICI in PDAC is often attributed to its unique tumor microenvironment (TME). This complex ecosystem drives tumor progression through mediating resistance to treatment and promoting metastatic spread and recurrence [13, 14]. Extensive profiling of the immune landscape of the human PDAC TME has revealed a complex environment of immunosuppressive cell populations and dysfunctional cytotoxic immune cells [15–17]. This intricate immune landscape facilitates immune evasion and tumor progression, making it a significant challenge for effective treatment. Within this context, the immune checkpoint TIGIT (T cell immunoreceptor with Ig and ITIM domains) has emerged as a critical modulator of immune suppression in PDAC [15, 16].

The TIGIT axis represents a complex regulatory pathway involving TIGIT, DNAM-1 (CD226), and TACTILE (CD96), which collectively modulate immune responses within the TME [18]. These receptors compete for shared ligands, including CD155 (PVR) and CD112 (NECTIN2), which play a central role in controlling immune activation and cytotoxicity. The balance between these receptors is crucial for immune regulation, with TIGIT generally outcompeting DNAM-1, thereby facilitating immune evasion [19]. Additionally, TACTILE functions as an inhibitory receptor that promotes tumor immune escape, further complicating immune regulation [18]. Until today, there are very few clinical trials that target TIGIT in PDAC patients (NCT05951608) and in some cases PDAC patients are even excluded from enrollment (NCT05757492).

The interplay between the TIGIT axis and PD-1 signaling introduces another layer of complexity [20]. Preclinical and clinical studies in various cancer types pointed out the potential of combined targeting of these pathways [21, 22]. However, in PDAC, the only clinical trial to date evaluating this combination strategy, conducted on a limited cohort, did not demonstrate therapeutic benefit [23]. While these findings are not definitive, they highlight the need for deeper exploration of the TIGIT axis to identify mechanisms of resistance and optimize future combination therapies. Therefore, this study aims to characterize key components of the TIGIT axis alongside PD-1/PD-L1 signaling in matched blood and tissue samples of PDAC patients.

Material and methods

Sample collection

Fresh tumor specimens were collected from pancreatic cancer patients who underwent surgical resection of the pancreatic tumor (Whipple procedure or distal pancreatectomy) at the Antwerp University Hospital. Tumor specimens were cut into 1–2 mm^3 tissue fragments, transferred in freezing medium (FBS + 10% DMSO), and stored in liquid nitrogen until further use. Additionally, paraffin-embedded tumor tissue fragments were obtained from resected specimen through the TumorBank@UZA.

During surgery, up to 50 mL of peripheral blood was collected in heparin tubes, for all patients consented. Peripheral blood mononuclear cells (PBMCs) were freshly isolated on the same day using Ficoll-Density centrifugation (GE Healthcare & Life Science). Isolated and washed PBMCs were resuspended in freezing medium (FBS + 10% DMSO) and stored in liquid nitrogen until further use. All human samples were obtained via Biobank Antwerp (Antwerp, Belgium, ID: BE 71030031000).

Flow cytometry

One day beforehand, PBMC and tumor tissue samples were thawed and rested overnight in PBMC medium (RPMI 1640 supplemented with 10% FBS, 2 mM L-glutamine, 100 U/mL penicillin, 100 µg/mL streptomycin, and 1 mM sodium–pyruvate) and 0.1 mg/mL DNase (Sigma-Aldrich) was added to prevent clumping of dead cells. On the day of staining, single-cell suspensions of tumor tissue fragments were obtained by enzymatic digestion using 2.5 mg/mL collagenase D (Sigma-Aldrich) and 0.2 mg/mL DNAse (Sigma-Aldrich) in PBMC medium, with gentle shaking at 37 °C for 1h, followed by filtration over a 100 µm strainer (Corning). PBMCs were harvested and washed with FACS buffer (PBS + 2% BSA + 1 mM EDTA).

Complete tumor tissue single-cell suspensions and 1 × 10E6 PBMCs per patient sample were used for staining. Prior to staining, all samples were blocked with 10% normal human serum (Sigma-Aldrich) in FACS buffer at 4 °C for 30 min. Next, all samples were stained with a cell-surface antibody cocktail in a 50 µL final volume. All antibodies and used dilutions are listed in Supplementary Table 1. Staining was carried out at 4 °C for 30 min.

Data acquisition was performed with the NovoCyte Quanteon (Agilent Technologies) flow cytometer. Data analysis was performed using FlowJo (RRID:SCR_008520) software (BD Biosciences) version 10.8.1 or higher. Gating strategy is depicted in Supplementary Fig. 1A-B. Samples with low

cell counts were excluded from analysis according to the flowchart in Supplementary Fig. 2B.

Immunohistochemistry staining

Paraffin-embedded tumor tissue samples were sectioned into 5-µm-thick slices and subjected to heat-induced antigen retrieval. This involved incubation in either a low-pH (pH 6) or high-pH (pH 9) buffer at 97 °C for 20 min, depending on the specific staining requirements. Subsequently, endogenous peroxidase activity was quenched by incubating the slides in peroxidase blocking buffer (DAKO) for 5 min. PD-L1 staining was performed with the PD-L1 IHC 22C3 pharmDx kit (DAKO/Agilent) according to manufacturer's instructions on an Omnis platform (Agilent). Other slides were manually stained with antibodies targeting CD155 (Cell Signaling Technology Cat# 81254, RRID:AB_2799970), CD112 (Sigma-Aldrich Cat# HPA012759, RRID:AB_1846227), CD111 (Santa Cruz Biotechnology Cat# sc-21722, RRID:AB_626865), and CD113 (Sigma-Aldrich Cat# SAB1402559, RRID:AB_10638278). The antibodies used and their dilutions are summarized in Supplementary Table 2. All stained samples were counterstained with hematoxylin. Whole slide images of stained sections were obtained with the Ultra-fast scanner 1.8 (Philips), using 40×objective. During export of images from the Phillips IntelliSite Pathology Solution, images were converted from ISyntax format to TIFF format. Further manipulations of the image were performed using Qupath. All stained slides were scored by an experienced pathologist.

Gene expression analysis

Gene expression data for PDAC were obtained from The Cancer Genome Atlas (TCGA) via the cBioportal portal. Expression values were provided in Transcripts Per Million (TPM) format and processed using RNA-Seq by Expectation–Maximization (RSEM) normalization. To compare gene expression between PDAC tumors and normal pancreatic tissue, Gene Expression Profiling Interactive Analysis 2 (Gepia2, RRID:SCR_026154) was used. This tool integrates expression data from TCGA (tumor) and GTEx (normal tissue) to provide standardized differential expression analysis. The tool was accessed at http://gepia2.cancer-pku.cn [24]. Fibroblast subtype data were obtained from published single-cell RNA sequencing data as described in the original publication [25]. The CAF subset classification and associated gene- expression matrices were used as provided. Visualization of ligand expression across fibroblast populations was generated using the Scanpy package in Python.

Sex as a biological variable

Sex was considered a biological variable in this study. We utilized human samples from both male and female PDAC patients and performed analyses to account for and evaluate sex-specific differences in our findings.

Data visualization and statistical testing

Student's *t* tests were used to compare experimental groups when all samples were matched (peripheral blood and tumor tissue). Normality was calculated using Shapiro–Wilk. If unmatched samples were included, a linear mixed-effect model was used. *P*-values of correlations were calculated using Spearman's or Pearson correlation as indicated. *P*-values < 0.05 were considered significant. Data- analysis was performed using GraphPad Prism (RRID:SCR_002798) version 10.0.0 or higher, Python (RRID:SCR_024202), and Gepia2. Data visualization was performed using Biorender (RRID:SCR_018361), GraphPad Prism (RRID:SCR_002798) version 10.0.0 or higher, Python (RRID:SCR_024202), and Gepia2.

Study approval and patient consent

This study was approved by the Ethics Committee of the University of Antwerp (Antwerp, Belgium) and the Antwerp University Hospital (Antwerp, Belgium) under the reference number 14/47/480. All patients enrolled in this study gave informed consent for the collection and use of tumor specimen and peripheral blood. All participants supplied material during surgery; therefore, no follow-up sample collection was required in this study, i.e., there was no attrition.

Results

Clinicopathological features of the PDAC patient cohort

The clinicopathological characteristics of the PDAC patient cohort in this study are summarized in Table 1 and Supplementary Fig. 2A. The cohort consisted of 25 male (70%) and 11 (30%) female patients, with a mean age of 65 years (50–80 years) at the time of surgery. Among these patients, 20% received neoadjuvant treatment with FOLFIRINOX, while the remaining patients received no prior treatment. Following surgery, adjuvant treatment was given to 64% of the patients, consisting of FOLFIRINOX or gemcitabine, either as monotherapy or in combination with capecitabine or nab-paclitaxel. The cohort included patients with tumor stages ranging from

Table 1 Demographics and clinical characteristics of enrolled PDAC patients. Gemcitabine (GEM), apecitabine (CAP), Nab-paclitaxel (NAB)

Patient characteristics (n = 36)		
Gender distribution		
Male	25	*(69.44%)*
Female	11	*(30.56%)*
Age at surgery (years)		
Mean ± SD	65.5 ± 8.7	
Stage distribution		
IA	1	*(2.78%)*
IB	6	*(16.67%)*
IIA	5	*(13.89%)*
IIB	13	*(36.11%)*
III	10	*(27.28%)*
Unknown	1	*(2.78%)*
Neoadjuvant treatment		
FOLFIRINOX	7	*(19.44%)*
None	29	*(80.56%)*
Adjuvant treatment		
No	12	*(33.33%)*
GEM	6	*(16.67%)*
GEM-CAP	10	*(27.78%)*
GEM-NAB	2	*(7.69%)*
FOLFIRINOX	5	*(13.89%)*
Unknown	1	*(2.78%)*
Resection status		
R0	27	*(75.00%)*
R1	8	*(22.22%)*
Unknown	1	*(2.78%)*
Metastasis occurring		
Yes	15	*(41.67%)*
No	3	*(8.33%)*
Unkown	17	*(47.22%)*
Lymph node invasion		
Yes	27	*(75.00%)*
No	8	*(22.22%)*
Unknown	1	*(2.78%)*
Neuroinvasion		
Yes	28	*(77.78%)*
No	6	*(16.67%)*
Unknown	2	*(5.56%)*

IA to III (according to the TNM classification UIC 8th edition [25]). Lymph node metastases were observed in 75% of the cases, and perineural invasion was identified in 78%. During post-operative follow-up, metastatic disease was recorded for 42% of patients. However, this information was unavailable for most of the cases (47%) due to follow-up in local non-academic hospitals.

Distinct immune cell subsets between peripheral blood and tumor tissue reflect the immunosuppressive tumor microenvironment

This study aimed to compare the composition of immune cell subsets between peripheral blood and tumor tissue in PDAC patients by using multiparametric flow cytometry and immune histochemistry (IHC) staining (Fig. 1A). Flow cytometry analysis revealed significant differences in various immune cell subtypes between these two compartments (Fig. 1B–F and Supplementary Fig. 3A), underscoring a distinct immune landscape within the TME of PDAC.

The overall frequency of $CD3^+$ T cells was significantly higher in tumor tissue than in peripheral blood (Fig. 1B). This is driven largely by a relative enrichment of specific T cell subsets. Within the $CD3^+$ population, $CD4^+$ T cells were significantly more abundant than $CD8^+$ T cells in both compartments, while the levels of both $CD4^+$ and $CD8^+$ T cells were markedly lower in PDAC tumor tissue compared to peripheral blood (Fig. 1B).

Further analysis of the $CD4^+$ T cell population revealed a significant shift in composition. While $CD4^+CD25^{int/high}CD127^{low}$ conventional regulatory T cells (Tregs) were almost absent in all peripheral blood samples, this cell population was significantly enriched in tumor tissue, exhibiting a high inter-patient variability in their distribution (Fig. 1B, D). This enrichment was accompanied by a pronounced increase in highly immunosuppressive HLA-DR^+ Tregs, highlighting the immune-suppressive nature of the TME (Fig. 1E). In contrast, $CD4^+CD25^-CD127^{high}$ non-regulatory T cells (non-Tregs) were significantly reduced in tumor tissue (Fig. 1D), further emphasizing the skewing of T cell populations toward immune suppression.

The most pronounced difference between compartments was observed in the $CD3^-CD56^+$ natural killer (NK) cells. These cytotoxic immune cells were markedly reduced in the tumors, with an average 14.5-fold lower frequency relative to peripheral blood (Fig. 1F) and a range of 3.7- to 51.8-fold across patients. Within the NK cell subsets, $CD56^{dim}$ NK cells, which are primarily associated with cytotoxicity, were statistically less prevalent in tumor tissue relative to blood (Fig. 1F). In contrast, $CD56^{bright}$ NK cells, which are predominantly linked to immune regulation, constituted a larger proportion of the NK cell population in tumor tissue compared to blood, reflecting a difference in the NK cell subset composition between these compartments.

Together, these observations indicate that Tregs and NK cells differ most prominently in frequency between peripheral blood and tumor tissue in PDAC.

Receptor modulation in tumor-infiltrating immune cells reveals TIGIT axis as a potential key mediator of PDAC immune evasion

To gain deeper insight into the expression profiles of the TIGIT axis, which might drive immune suppression in PDAC, we examined the expression of its key immune receptors—TIGIT, DNAM-1, and TACTILE—across various lymphocyte populations from peripheral blood and tumor tissue (Fig. 2). Notably, the inhibitory receptor TIGIT is consistently higher expressed across all tumor-infiltrating lymphocyte subtypes (Fig. 2A, D, Supplementary Fig. 3B), both in terms of mean fluorescence intensity (MFI) per cell and the frequency of TIGIT-positive cells. Among all analyzed subsets, Tregs exhibit the highest TIGIT expression, both systemic and within the tumor (Fig. 2A). Given that TIGIT functions as an inhibitory receptor on cytotoxic cells including NK and $CD8^+$ T cells, its elevated expression on Tregs enhances their immunosuppressive capacity [26]. Furthermore, the induced TIGIT expression on $CD8^+$ T cells and NK cells underscores the suppression of their cytotoxic activity, reinforcing the immune evasion mechanisms present in the PDAC TME.

In contrast, the expression of the activating receptor DNAM-1 shows a marked decrease within the TME across most investigated immune cell subtypes, with the most pronounced reductions observed in NK cells (Fig. 2B, D, Supplementary Fig. 3B). Furthermore, the frequency of DNAM-1^+ $CD8^+$ T cells and DNAM-1^+ NK cells is significantly diminished in the PDAC tumor, further underscoring the immune-suppressive nature of the PDAC TME (Fig. 2B). Notably, Tregs are the only immune cell type that exhibits a significant upregulation of DNAM-1, which is even more pronounced on the highly immunosuppressive HLA-DR^+Tregs. These findings again demonstrate the immunosuppressive landscape of PDAC, also by downregulation of activating receptors.

Finally, TACTILE is expressed by almost all analyzed immune cell types, both in peripheral blood and tumor-infiltrating lymphocytes (Fig. 2C and Supplementary Fig. 3B). Notably, within the NK- cell subtypes, TACTILE was largely restricted to $CD56^{bright}$ NK cells. In peripheral blood, approximately 78% of $CD56^{bright}$ NK cells expressed TACTILE, whereas expression was only detected in 10% of the $CD56^{dim}$ NK cells. In general, changes in TACTILE expression between peripheral blood and tissue were comparatively modest (Fig. 2D), except for $CD56^{dim}$ NK cells of which approximately 10% expressed TACTILE in peripheral blood (Fig. 2C–D). The most notable intratumoral enrichment of TACTILE expression is observed on Tregs. Specifically, HLA-DR^+ Tregs show the largest increase of TACTILE within the TME (Fig. 2C, D).

Taken together, the differential expression of TIGIT, DNAM-1, and TACTILE across immune cell subsets underscores the complexity and heterogeneity of receptor expression profiles in PDAC. While further functional validation is required, these findings underline the potential of targeting TIGIT to overcome immune suppression in PDAC patients.

Intratumoral regulatory T cells display enriched co-expression of TIGIT axis receptors in PDAC

Because TIGIT axis receptors share ligands with different affinities, we examined their co-expression patterns to define how these receptors are distributed across immune subsets. To characterize co-expression patterns of the TIGIT axis in peripheral blood and PDAC tissue, we analyzed the combined expression of DNAM-1, TACTILE, and TIGIT (Fig. 3 and Supplementary Fig. 3C). In peripheral blood, triple co-expression of these receptors was nearly absent (< 4%) across all systemic T cell subsets, with the exception for HLA-DR^+ Tregs in which approximately 8% of the cells exhibited triple positivity (Fig. 3A). Across all analyzed populations, the highest frequency of intratumoral triple-positive cells was observed in Tregs, and more specifically in the highly immunosuppressive HLA-DR^+ Tregs, where 29% of the cells displayed all three receptors (Fig. 3A, B). In contrast, intratumoral $CD8^+$ T cells more frequently lacked expression of all three receptors, as evidenced by the significant enrichment of DNAM-1^-TACTILE$^-$TIGIT$^-$ $CD8^+$ T cells within the tumor tissue (Fig. 3A, B). In contrast, Tregs within the TME rarely exhibit this triple-negative phenotype, suggesting their ability to retain higher levels of receptor expression in the suppressive milieu of the tumor (Fig. 3A). Additionally, DNAM-1^+TACTILE$^-$TIGIT$^-$ T cell subtypes are also more prevalent within peripheral blood, yet this population undergoes a substantial reduction across all T cell subsets within the TME with the most striking loss observed in $CD8^+$ T cells and non-Treg populations.

Although these co-expression patterns do not imply functional regulation or causal relationships, they describe differences in TIGIT axis-related receptor co-expression across distinct T cell subtypes in the TME of PDAC.

DNAM-1 expression patterns correlate with NK cell presence in PDAC

Differences in the expression patterns of DNAM-1, TACTILE, and TIGIT between peripheral blood and PDAC tissue

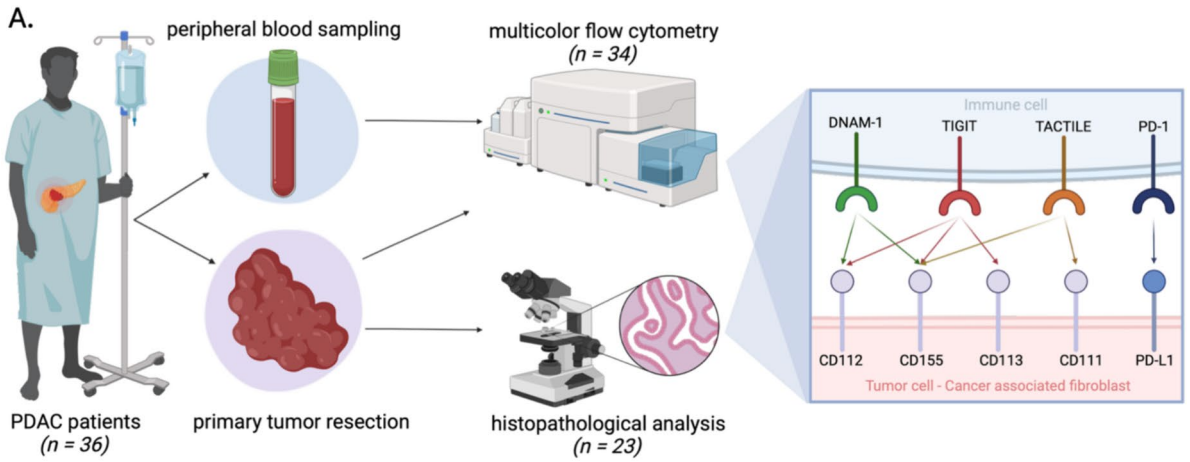
A.
peripheral blood sampling
multicolor flow cytometry
(n = 34)
Immune cell
DNAM-1
TIGIT
TACTILE
PD-1
CD112
CD155
CD113
CD111
PD-L1
Tumor cell - Cancer associated fibroblast
PDAC patients
(n = 36)
primary tumor resection
histopathological analysis
(n = 23)


Confirmed PDAC
Flow cytometry
Immunohistochemistry
yes
no

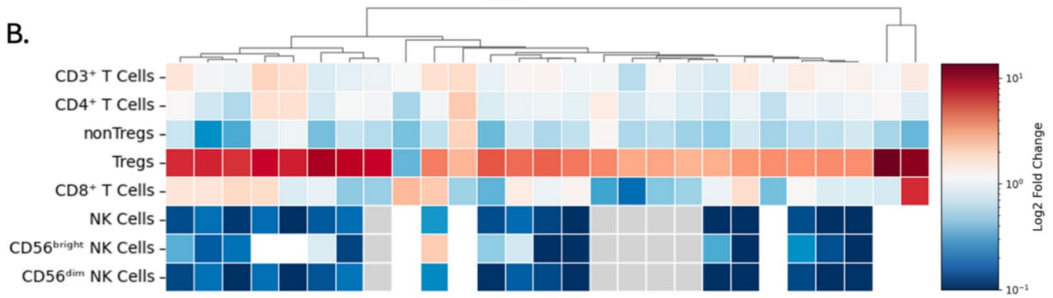
B.
CD3⁺ T Cells
CD4⁺ T Cells
nonTregs
Tregs
CD8⁺ T Cells
NK Cells
CD56bright NK Cells
CD56dim NK Cells
Log2 Fold Change

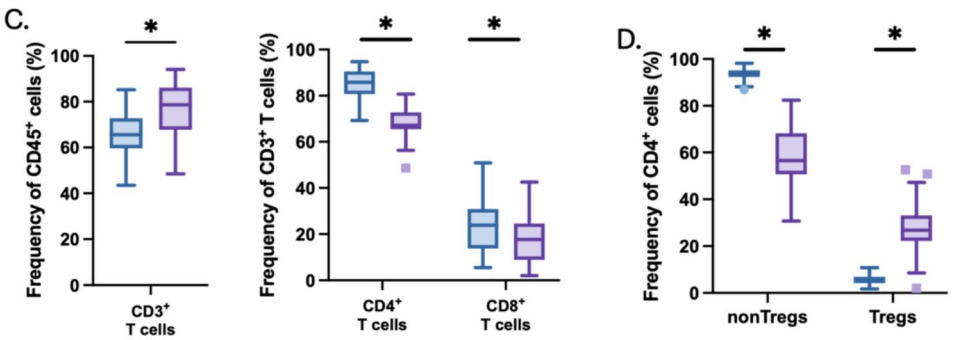
C.
Frequency of CD45⁺ cells (%)
CD3⁺ T cells
Frequency of CD3⁺ T cells (%)
CD4⁺ T cells
CD8⁺ T cells
D.
Frequency of CD4⁺ cells (%)
nonTregs
Tregs

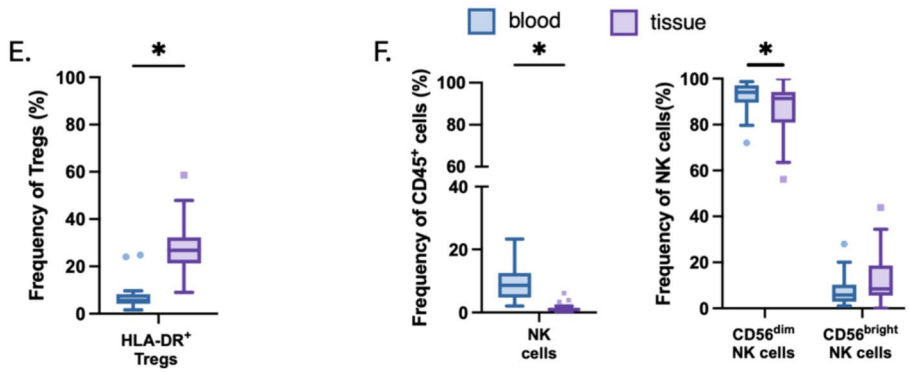
blood
tissue
E.
Frequency of Tregs (%)
HLA-DR⁺ Tregs
F.
Frequency of CD45⁺ cells (%)
NK cells
Frequency of NK cells(%)
CD56dim NK cells
CD56bright NK cells

◂**Fig. 1** The blood to tumor lymphocyte landscape in PDAC transitions to immunoregulatory subsets. **A** Schematic representation of the study set-up. A total of 36 patients with PDAC tumors were included in the study. Matched blood and tissue samples were taken on the day of the surgical procedure. Samples were processed using multiparametric flow cytometry and/or immunohistochemistry (IHC) to analyze immune cell subsets and the expression of receptors and ligands related to the TIGIT axis. The lower panel shows an overview of patients analyses, indicating which patients (columns) underwent flow cytometry and/or IHC analysis. Light green squares represent patients included in the analysis, while dark shaded squares indicate exclusion. **B** Clustered heatmap showing the log2 fold changes in immune cell subsets between blood and tumor tissue per patient (columns) calculated using the frequency among total immune cells ($CD45^+$ cells). Rows represent immune cell subsets. Blue indicates a decrease, and red indicates an increase in tumor tissue compared to blood. Gray boxes mark the subsets that were excluded due to low immune cell counts. Dendrogram represents hierarchical clustering. (C–F) Boxplots (Tukey) represent the frequency of lymphocyte subsets in peripheral blood (blue) versus tumor tissue (purple). The data are represented by frequency of parent. **C** Frequency of $CD3^+$ (left panel) and $CD4^+$ and $CD8^+$ (right panel) T cells in blood versus tumor. **D** Frequency of $CD4^+$ T cell subsets, including $CD25^-CD127^{high}$ non-regulatory $CD4^+$ T cells (nonTregs) and $CD4^+CD25^{int/high}CD127^{low}$ regulatory T cells (Tregs). **E** Frequency of HLA-DR^+ Tregs in blood versus tissue. **F** Frequency of NK cells within the $CD45^+$ population (left panel) and the distribution of $CD56^{dim}$ and $CD56^{bright}$ NK cell subsets. Statistical analysis was performed using a linear mixed-effect model to compare blood and tissue samples. Significance is indicated by asterisks (*), with *p*-values < 0.05 considered statistically significant

were also evident for NK cells (Fig. 3C, D). Specifically, there was a significant increase in NK cells lacking DNAM-1 expression within the tumor (Fig. 3D). This was observed for both $CD56^{bright}$ and $CD56^{dim}$ subtypes. Given the significant lack of NK cells within the PDAC tumor (Fig. 1F), we next examined the relationship between NK cell infiltration and their DNAM-1 expression. Correlation analysis revealed an inverse association between DNAM-1 expression on NK cells and their abundance within the tumor tissue (Fig. 3E). Similarly, the proportion of DNAM-1^+ NK cells negatively correlated with overall NK cell infiltration. In contrast, DNAM-1^-TACTILE$^+$TIGIT$^+$ NK cells showed a positive correlation with increased NK cell infiltration (Supplementary Fig. 3D).

To assess potential clinical associations, exploratory analyses revealed no significant association between DNAM-1 MFI on tumor-infiltrating NK cells and overall survival or disease stage (Supplementary Fig. 4A and B). In contrast, DNAM-1 MFI was significantly higher in tumors with perineural invasion, while no difference was observed with respect to lymphovascular invasion (Supplementary Fig. 4C and D).

Importantly, these associations do not establish causality, and reduced DNAM-1 expression might also be a consequence of sustained ligand exposure. Supporting the latter possibility, analysis of TCGA datasets further revealed a significant inverse correlation between DNAM-1 expression and CD112, but not CD155 (Fig. 3F). Given that high expression of these ligands in the TME might lead to DNAM-1, downregulation suggests a mechanism by which tumors could actively suppress DNAM-1 expression to evade immune surveillance. Collectively, these data underscore the context-dependent nature of DNAM-1 expression within the TME of PDAC.

Coordinated expression of TIGIT axis ligands CD112 and CD155 in PDAC

Building on the observed expression patterns of TIGIT axis receptors in immune cells, we focused on its key ligands: CD155, CD112, CD111, and CD113. These ligands interact with various receptors of the TIGIT axis and may therefore play a critical role in immune evasion (Fig. 1A). To investigate their expression and spatial distribution we performed IHC analysis (Fig. 4). Unfortunately, CD113 staining was not suitable for scoring (Supplementary Fig. 5A), limiting our analysis to CD155, CD112, and CD111. IHC staining revealed a clear presence of these ligands within the PDAC TME (Fig. 4A). Among them, CD155 and CD112 were significantly more abundant than CD111 (Fig. 4B). CD155 exhibited the highest expression among tumor cells, with substantial inter-patient variability. CD112, in contrast, showed moderate tumor expression, with similar variability observed across the cohort (Fig. 4B). Notably, CD112 also displayed stromal staining in 25% of patients (Supplementary Fig. 5C).

To complement these protein-level findings, we analyzed RNA expression data from TCGA (tumor) and GTEx (normal pancreas). CD155, CD112, and CD113 were significantly upregulated in PDAC tumors compared to normal pancreatic tissue (Supplementary Fig. 6A). CD111 also showed an increase, although not statistically significant. Additionally, PDAC demonstrated among of the most pronounced differences in CD112 and CD155 expression between tumor and normal tissue (Supplementary Fig. 6B). At protein level, CD112 and CD155 tended to increase with tumor stage, although this trend did not reach statistical significance ($p = 0.066$ Fig. 4C). Interestingly, this increase was not reflected at the transcriptional level (Supplementary Fig. 6C).

Finally, we observed a positive correlation between CD112 and CD155 expression, both at the protein and the transcriptional level (Fig. 4D–E, Supplementary Fig. 6D). This correlation even became stronger as tumor stage increased (Supplementary Fig. 6E).

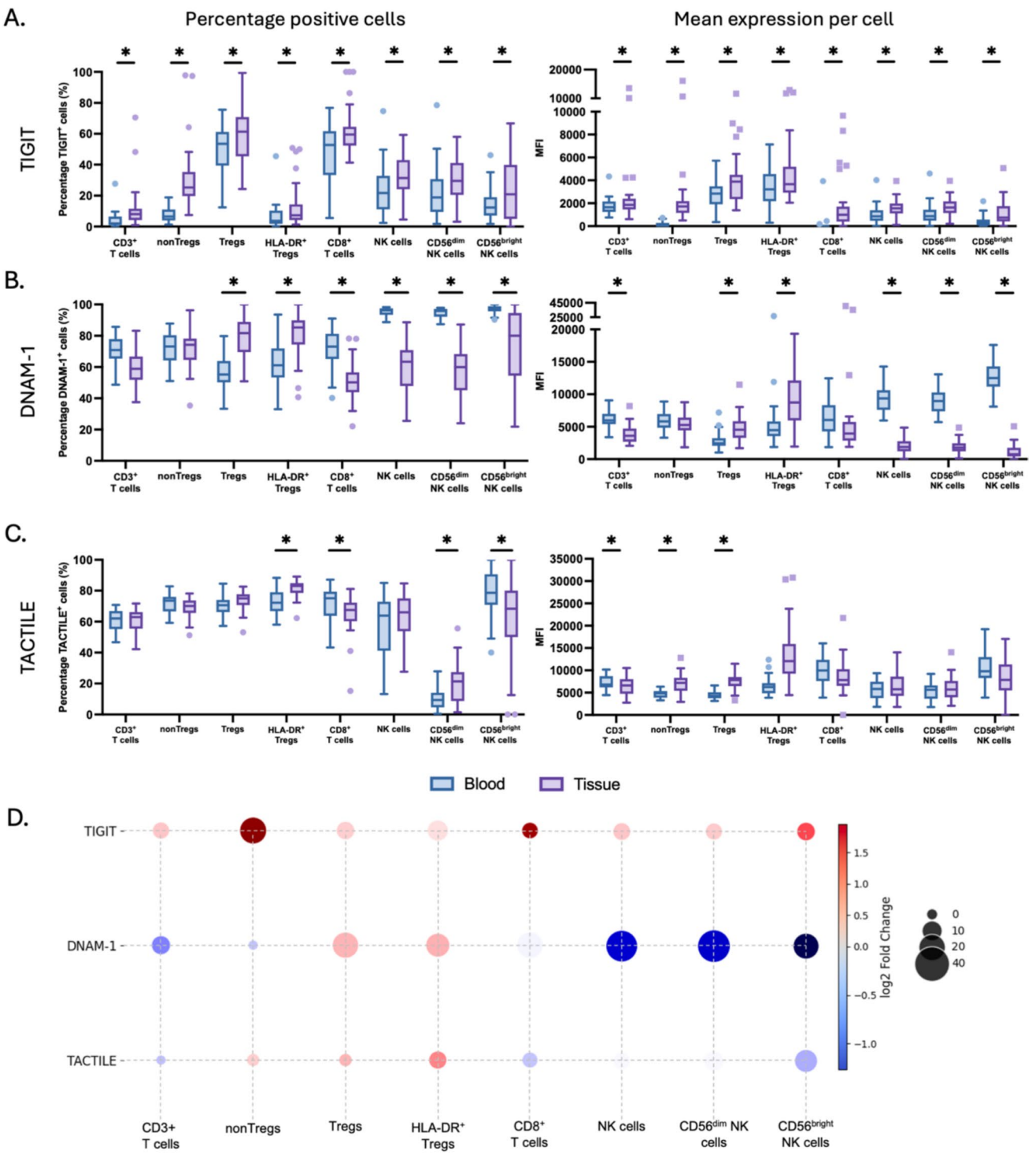

Fig. 2 Expression of receptors of the TIGIT axis on PDAC-infiltrating versus systemic lymphocytes are skewed toward immunosuppression **A–C** Boxplots (Tukey) comparing the expression of the immune receptors TIGIT, DNAM-1, and TACTILE on lymphocyte subsets from peripheral blood (blue) and tumor tissue (purple). Data are shown as both the percentage of positive cells (left panel) and the mean fluorescence intensity (MFI) per cell (right panel). Statistical significance is denoted by * ($p < 0.05$), determined using linear mixed-effect models. **D** Bubble heatmap illustrating the differential expression of receptors on tumor-infiltrating versus peripheral blood lymphocyte subsets. Bubble size reflects the absolute difference in the percentage of positive cells. The color gradient represents the fold-change in MFI when comparing tissue to blood, with red indicating an increase and blue indicating a decrease in the tumor

Together, these findings show the prominent role of CD155 and CD112 in PDAC, both in terms of abundance within the TME and their correlation with tumor progression. These data further support the idea that these ligands jointly contribute to immune evasion in PDAC via the TIGIT axis and support further investigation into its potential to serve as a therapeutic target.

TIGIT expression is correlated to PD-1 expression on T cells in PDAC tumors

Co-expression of inhibitory receptors such as PD-1 and TIGIT on immune cells is a hallmark of immune exhaustion, often associated with impaired antitumor responses. In clinical trials, monoclonal antibodies targeting TIGIT are frequently administered in combination with PD-(L)1 checkpoint inhibitors to enhance immune activation and reinvigorate exhausted T cells and restore antitumor immunity. This provides a rationale to examine the co-expression of the receptor across lymphocyte subsets in both peripheral blood and PDAC tumor tissue as well as the PD-L1 expression in the TME (Fig. 5 and Supplementary Fig. 7).

In peripheral blood, the majority of T cells predominantly exist in a PD-1^{-}TIGIT-state (Fig. 5A), with TIGIT expression largely restricted to regulatory T cells (Tregs). However, within the TME, there is significant upregulation of PD-1 across all T cell subsets, leading to a marked increase in both PD-1^{+}TIGIT^{+} and PD-1^{+}TIGIT^{-} intratumoral T cell populations (Fig. 5B). Notably, PD-1 and TIGIT expression was strongly correlated in both circulating and intratumoral T cells (Supplementary Fig. 7B), suggesting a potential benefit for co-targeting these pathways to reverse immune suppression. Within the tumor, this correlation was consistently observed across all CD4^{+} subsets, including non-Tregs, conventional Tregs, and immunosuppressive HLA-DR^{+} Tregs. However, this co-expression pattern was absent in CD8^{+} T cells within the PDAC tumor.

For NK cells, a similar trend was observed, where systemic NK cells, including both CD56^{dim} and CD56^{bright} NK cells, rarely express TIGIT or PD-1 (Fig. 5C). In contrast, intratumoral NK cells displayed a significant increase in PD-1^{+}TIGIT^{+} and PD-1^{+}TIGIT^{-} populations (Fig. 5C, D). However, unlike on T cells, PD-1 and TIGIT expressions on NK cells were not strongly correlated, neither in the tumor nor in peripheral blood (Supplementary Fig. 7C).

Although the widespread PD-1 expression is high across all intratumoral lymphocytes, PD-L1 expression in PDAC tumors remains strikingly low, both on cancer cells and immune cells (Fig. 5E). Additional complementary analysis of TCGA data indicated an increase in PD-L1 expression, compared to normal pancreatic tissue, although not significant (Supplementary Fig. 7D). This increase is not correlated with either CD112 or CD155 (Supplementary Fig. 7E). This raises critical questions about the true efficacy of PD-1 blockade in PDAC, given that PD-1 inhibitors rely on PD-L1 engagement to disrupt immune suppression.

Discussion

PDAC is one of the most aggressive and therapy-resistant cancers, characterized by its dense stromal architecture and complex immune microenvironment. A key challenge in treating PDAC is the tumor's ability to evade immune surveillance, particularly through the suppression of cytotoxic immune responses [27]. ICI targeting the PD-1/PD-L1 and CTLA-4 axes has revolutionized cancer treatment in other malignancies, yet their efficacy in PDAC has been limited [28]. Recent studies have shifted focus to the TIGIT axis, a critical immune checkpoint involved in the regulation of immune responses [29]. TIGIT, along with its ligands CD155 and CD112, plays a crucial role in immune suppression within the TME. This has also been confirmed in PDAC in a murine model [15, 16]. Understanding how TIGIT contributes to immune evasion in PDAC is essential for developing more effective immunotherapies for this deadly cancer. Therefore, in this study we performed a comprehensive protein-level characterization of key immune checkpoint receptors and ligands in PDAC patients' peripheral blood and matched tissue samples, with a focus on the TIGIT and PD-1/PD-L1 axis, which can inform future immunotherapeutic strategies.

The clinicopathological characteristics of our PDAC patient cohort offer valuable insights into the study population. Our cohort included 36 PDAC patients undergoing surgical resection, with a male predominance (70%) with a median age of 65 years, aligning with prior reports of higher PDAC incidence in males [30, 31]. High rates of lymph node metastases (75%) and perineural invasion (78%) confirm the aggressive nature of PDAC, reinforcing their role as prognostic markers of poor survival outcomes [32, 33]. While our sample size was limited, the inclusion of TCGA data helped to complement key expression patterns across a broader cohort, strengthening the reliability of our findings. A key limitation to both our study and TCGA data is the underrepresentation of late-stage tumors, which are ineligible for surgical resection. It would be interesting for future studies to focus on larger cohorts with more advanced-stage tumors and comprehensive follow-up.

Consistent with previous reports, our study demonstrates that the immune landscape of PDAC is profoundly immunosuppressive, with a deficiency of cytotoxic immune cells and an overrepresentation of immunosuppressive

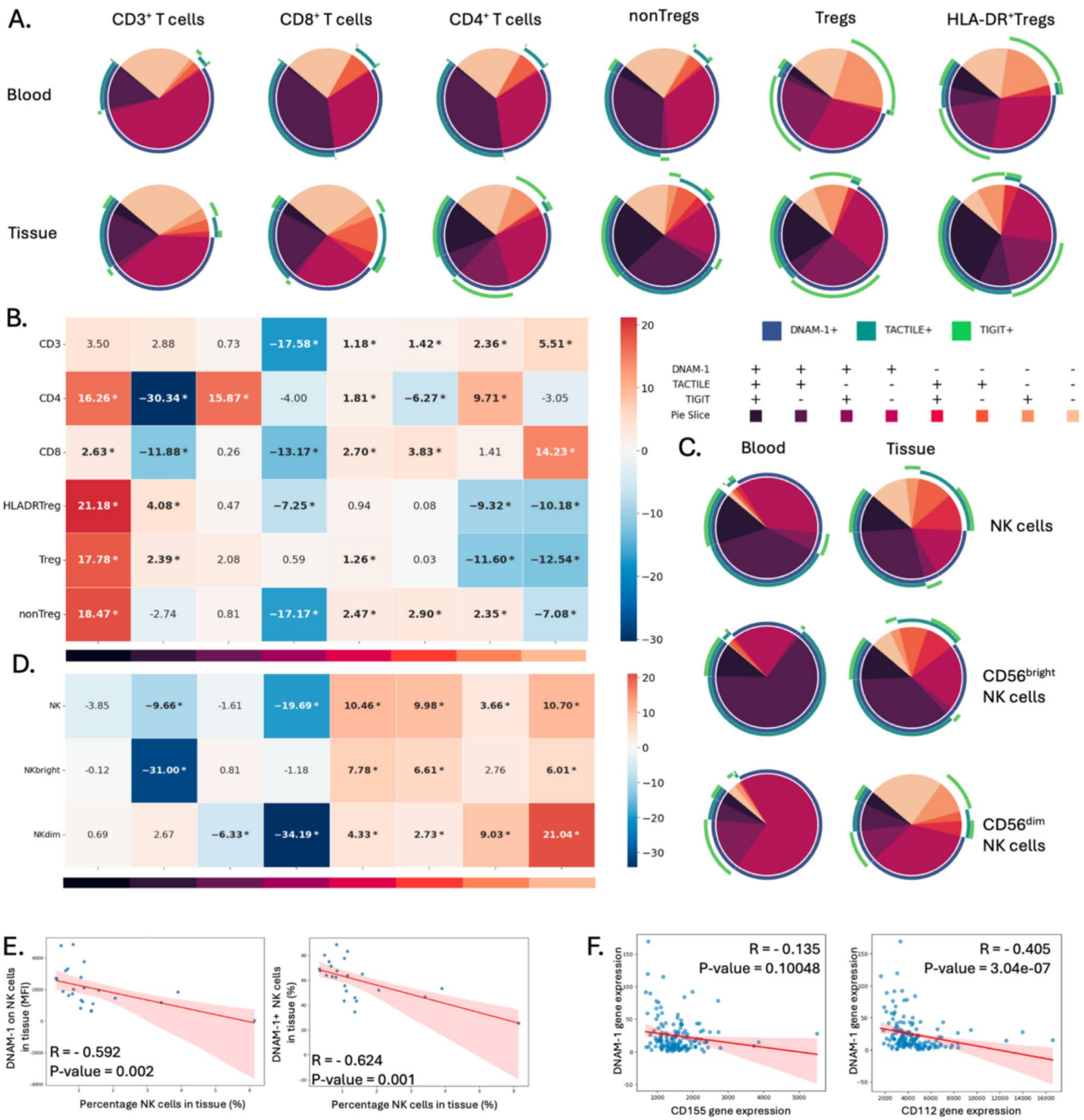

populations. For the T cell compartment, the overall proportion of CD8$^+$ T cells was significantly reduced in tumor tissue, which aligns with prior studies showing CD8$^+$ T cell depletion in the PDAC TME compared to circulation or normal pancreatic tissue [34, 35]. On the other hand, our analysis revealed a substantial intratumoral increase of Tregs, a finding that is well-supported by existing literature [36]. The abundance of Tregs in PDAC tumors could be linked to disease progression and poor patient survival [36]. Additionally, the CD8$^+$/Treg ratio has been correlated with response in melanoma patients treated with anti-PD-L1 therapy [37]. However, this relationship remains controversial, as one study reported no significant difference in the CD8$^+$/Treg ratio between responders and non-responders treated with anti-PD-1 therapy in gastric cancer, advanced melanoma or non-small cell lung cancer [38]. To our knowledge, we are the first to report an increase in HLA-DR$^+$ Tregs within the PDAC TME compared to

◂**Fig. 3** Co-expression of DNAM-1, TACTILE, and TIGIT is correlated with NK cell infiltration in PDAC tumors. **A** Pie charts illustrating the proportion of T cell subsets expressing DNAM-1, TACTILE, and/or TIGIT. For each subset, pie charts represent cells from peripheral blood (upper row) and tissue (lower row). Pie segments and arcs are color-coded to indicate the expression categories: DNAM-1$^+$ (dark blue arcs), TACTILE$^+$ (dark green arcs), TIGIT$^+$ (light green arcs), and combinations thereof as defined in the legend below. **B** Heatmap depicting the absolute difference per T cell subset expressing DNAM-1, TACTILE, and/or TIGIT. The color bar represents the absolute difference in percentage, with decrease (blue) and increase (red) in the tumor. Statistical significance was determined using a linear mixed-effects model. Benjamini-Hochberg correction was applied to adjust *p*-values. Adjusted *p*-values < 0.05 were considered significant and depicted in bold with an *. **C** Pie charts illustrate the proportion of NK cell subsets expressing DNAM-1, TACTILE, and/or TIGIT. The same color legend was used as in A. **D** Heatmap depicting the absolute difference per NK cell subset expressing DNAM-1, TACTILE, and/or TIGIT. The color bar represents the absolute difference in percentage, with decrease (blue) and increase (red) in the tumor. Statistical significance was determined using a linear mixed-effects model. Benjamini–Hochberg correction was applied to adjust *p*-values. Adjusted *p*-values < 0.05 were considered significant and depicted in bold with an *. **E** Correlation analysis depicting association between the expression of DNAM-1 and NK cell infiltration in PDAC tissue samples. The left panel shows the correlation between the proportion of DNAM-1$^+$ NK cells expressed by the frequency of CD45$^+$ cells (FOCD45). The right panel shows the correlation between geometric mean of DNAM-1 on NK cells. Data points represent individual samples, with the red line indicating the best-fit linear regression and the shaded area representing the confidence interval. Spearman correlation coefficients (*R*) and *p*-values are depicted. **F** Correlation analysis depicting association between the gene expression of DNAM-1 and CD155 (left panel) or CD112 (right panel) obtained from TCGA data from PDAC patients. Data points represent individual samples, with the red line indicating the best-fit linear regression and the shaded area representing the confidence interval. Spearman correlation coefficients (*R*) and *p*-values are depicted

peripheral blood. HLA-DR, a marker of Treg activation, suggests that HLA-DR$^+$ Tregs possess enhanced immunosuppressive properties compared to their HLA-DR$^-$ counterparts, evidenced by increased FoxP3 expression and functional stability [39, 40]. These findings provide novel insights into the role of activated Tregs in PDAC and their potential contribution to immune suppression within the TME.

In addition to adaptive immune alterations, our data strengthen the notion that innate immune surveillance is compromised in PDAC as tumor-infiltrating NK cells were scarce within the PDAC TME. These low numbers are in line with recent studies on NK cell presence in PDAC [41, 42]. Specifically, the cytotoxic CD56^{dim} NK cell subset was significantly diminished in tumor tissue compared to peripheral blood, whereas the immunoregulatory CD56^{bright} NK cells were more prevalent. This shift in NK cell composition illustrates the functional impairment of innate immune responses within the TME and emphasize the need for therapies aimed at restoring NK cell cytotoxicity to enhance immune-mediated tumor control in PDAC.

Within this context, we examined expression patterns of the TIGIT axis receptors on NK cells and observed a significant inverse correlation between DNAM-1 expression and NK cell presence within the PDAC TME. While these associations do not establish causality, they suggest a relationship between DNAM-1 expression status and NK cell distribution within PDAC tumors. One possible explanation is that reduced DNAM-1 expression may contribute to impaired NK cell infiltration, as previous research found that DNAM-1-deficient NK cells exhibit minimal motility capacities [43] and its pivotal role in monocyte migration [44]. However, this hypothesis requires further functional validation.

DNAM-1 plays a central role in NK-cell activation and is crucial for degranulation and killing activity against cancer cells expressing its ligands CD112 or CD155 [45, 46]. Notably, DNAM-1 expression is dynamically regulated by ligand engagement. Chronic exposure to its ligands CD112 and CD155 has been shown to drive DNAM-1 downregulation [47]. Recent mechanistic studies have demonstrated that this loss is regulated through post-translational mechanisms upon increasing ligand density on target cells [48]. These findings underscore the importance of assessing the receptor on the protein level and highlight a potential avenue for therapeutic strategies aimed at restoring or maintaining DNAM-1 expression.

In addition to its downregulation on NK cells, DNAM-1 is also downregulated on cytotoxic CD8$^+$ T cells, further underlining the immunosuppressive nature of the PDAC TME. Interestingly, a contrasting pattern emerges with Tregs, which uniquely upregulate DNAM-1 in the PDAC TME. This observation stands in contrast with previous reports in melanoma, where intratumoral Tregs exhibited reduced DNAM-1 expression [49]. While DNAM-1 signaling is known to enhance the activation of cytotoxic immune cells, its role on Tregs remains controversial. In vitro studies have linked DNAM-1 loss in Tregs to both enhanced and loss of immunosuppressive activity [50, 51]. This exposes the complexity of its function in this subset. Further mechanistic studies will be essential to validate how DNAM-1 expression influences Treg behavior and its contribution to shaping the immune TME in PDAC.

In contrast to DNAM-1, our data show TIGIT overexpression across multiple immune cell subsets, with the highest expression observed on Tregs. Given the role of TIGIT in enhancing Treg immunosuppressive function, this upregulation likely reinforces immune evasion in the PDAC TME [26]. Additionally, TIGIT upregulation was also observed on cytotoxic CD8$^+$T cells, which is associated with T cell

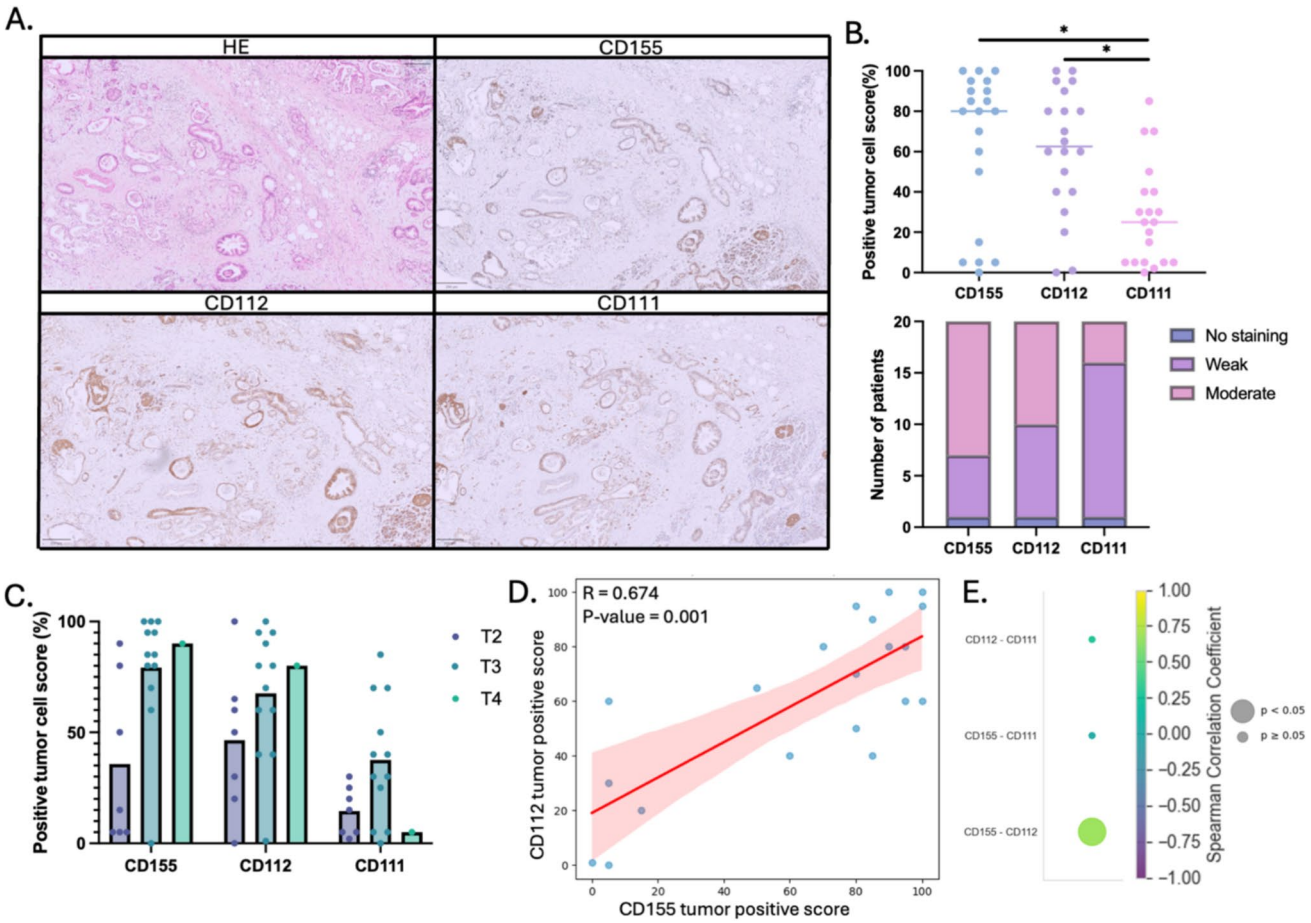

Fig. 4 High CD155 and CD112 co-expression among nectin family ligands suggests immune evasion via the TIGIT axis in PDAC **A** Representative histological images of tumor tissue stained with hematoxylin and eosin (HE) and immunohistochemistry staining for CD155, CD112, and CD111. **B** Dot plots quantifying the percentage of positive tumor cell scores (%) for CD155, CD112, and CD111. Each dot represents the percentage of positive tumor cells in individual samples, with horizontal lines indicating the mean value Shapiro–Wilk test was used to assess normality, and Friedman test was used to determine statistical significance between groups, $p < 0.05$ was considered significant. **C** Bar plot showing the mean positive tumor cell scores (%) for CD155, CD112, and CD111 across different tumor stages. Each dot represents an individual sample. **D** Correlation plot illustrating the correlation between CD112 and CD155 ligand expression determined by immune histochemistry. Each data point represents an individual sample, with the red line indicating the best-fit linear regression and the shaded area representing the confidence interval. Spearman correlation coefficients (R) and p-values are depicted. **E** Heatmap bubble plot displaying the correlation between ligand expression levels. The color intensity represents the Spearman correlation coefficient, while bubble size indicates the statistical significance, as shown in the color legend

dysfunction and reduced cytotoxic capacity toward cancer cells [52]. Our findings align with previous research in PDAC, where TIGIT expression was elevated on intratumoral $CD8^+$ T cells and was correlated with features of exhaustion, including reduced cytokine production and impaired tumor-reactive functionality [15, 53]. This observation is further supported by prior work showing that TIGIT-CD155 signaling contributes to dysfunctional antitumor T-cell activity in PDAC models, reinforcing the relevance of this axis in shaping intratumoral T-cell exhaustion [16].

To further elucidate the role of the TIGIT axis in PDAC, we focused on its ligands, CD155, CD112, and CD111, known to interact with TIGIT to facilitate immune evasion. IHC analysis revealed varying expression patterns for these ligands within the PDAC TME. Among them, CD155 and CD112 exhibited the highest expression on tumor cells, consistent with previous studies linking high CD155 and CD112 expression to poor survival prognosis in PDAC [54, 55]. Notably, we also observed stromal CD112 staining in fibroblast for 25% of PDAC patients, which was also confirmed on transcriptional level, demonstrating the predominant expression in myCAFs. To our knowledge, this is the first report of stromal CD112 expression in PDAC, which may indicate that CD112 may contribute to fibroblast-mediated

immune suppression within the TME. In colorectal cancer, $CD112^+$ cancer-associated fibroblasts (CAFs) were identified as a novel subtype. These experiments point out the functional impact of $CD112^+$ CAFs on T cell functionality by reducing their proliferation and increasing exhaustion [56].

The mechanistic convergence of TIGIT and PD-1 has been demonstrated in preclinical models, where dual blockade of PD-1 and TIGIT restored DNAM-1 signaling, leading to enhanced cytotoxic T cell activity and anti-tumor activity [20]. Additionally, one study showed that targeting TIGIT in combination with PD-1 blockade and CD40 agonist restored antitumor T cell response in a murine PDAC model [16]. This suggests that blocking either PD-1 or TIGIT alone is insufficient to fully restore anti-tumor immunity, as both pathways act in an independent manner to suppress DNAM-1–mediated activation of cytotoxic T cells. In this context, our data describe expression patterns relevant to this axis in human samples. We observed a strong correlation between TIGIT and PD-1 expression on $CD3^+$ T cells in both peripheral blood and tumor tissue. While PD-1 expression was low across all circulating lymphocyte subsets, tumor-infiltrating lymphocytes exhibited a significant increase in PD-1 and TIGIT co-expression, consistent with previous studies linking that PD-1/TIGIT co-expression to immune exhaustion in PDAC [53]. These findings align with previous studies showing that TIGIT is the only immune checkpoint receptor that is consistently overexpressed on tumor-infiltrating $CD8^+$ T cells when compared to adjacent normal tissue, further reinforcing its critical role in shaping T cell dysfunction [15].

Despite the widespread PD-1 expression on intratumoral lymphocytes, PD-L1 expression remained low in PDAC tumor tissue, consistent with prior reports. Given the low PD-L1 expression observed in the PDAC tumor, the limited clinical efficacy of PD-1 blockade alone remains a significant challenge. Analysis of TCGA datasets suggested a modest, non-significant increase in PD-L1 expression relative to normal pancreatic tissue, which did not correlate with expression of CD112 or CD155. Together, these observations may help contextualize the limited clinical efficacy of PD-1/PD-L1 blockade observed in PDAC, although conclusions regarding therapeutic responsiveness cannot be drawn, as treatment outcomes were not evaluated in this study.

Importantly, studies have proven that PD-L1 expression alone might not be the ideal predictor of response to PD-1–targeted therapies. For example, PD-L1 levels did not differ significantly between responders and non-responders in malignant pleural mesothelioma [57] and alternative parameters, including the spatial proximity of $CD8^+$ T cells to tumor cells and the absence of Tregs predicts the response. Additionally, the ratio of $PD\text{-}1^+CD8^+$ cells/$PD\text{-}1^+$ Tregs in the TME was proven to be a superior predictor of clinical efficacy for PD-1 blockade therapies compared to other biomarkers such as PD-L1 expression [38]. While these findings derive from other cancer types, they suggest that immune cell-intrinsic features might be relevant determinants of response to PD-1-targeted therapies in PDAC as well.

A limitation of this study is that functional assays assessing immune cell activity were not performed, precluding direct conclusions regarding immune exhaustion or cytotoxic capacity. Furthermore, although complementary transcriptional analyses were included, discrepancies between mRNA and protein expression highlight the importance of protein-level analyses and underscore the need for integrated, multi-level approaches in future studies. Although the limited cohort size restricts the identification of prognostic associations, the detailed protein-level characterization presented here provides clinically relevant insight into the inhibitory receptor–ligand landscape that may contribute to the limited efficacy of checkpoint therapies in PDAC. These expression patterns, defined directly in human tumors, offer a foundation for future studies exploring TIGIT-directed or combination immunotherapeutic strategies.

In summary, this study provides a detailed protein-level characterization of TIGIT-axis receptors and ligands in human PDAC, revealing distinct expression patterns across immune subsets and between peripheral blood and tumor tissue. Our findings emphasize the complexity of immune checkpoint regulation in PDAC and highlight the importance of studying these pathways directly in human tumors. This work provides a framework for future functional and longitudinal studies aimed at clarifying how TIGIT-axis components and related immune features shape antitumor immunity and influence responses to immunotherapeutic strategies in PDAC.

Conclusion

In conclusion, our study identifies the TIGIT axis as a pivotal component of the PDAC TME. Widespread upregulation of TIGIT and downregulation of DNAM-1 on various lymphocytes in the TME of PDAC, along with overexpression of their ligands CD155 and CD112, contribute to the immunosuppressive landscape. Co-expression of PD-1 and TIGIT further enhances intratumoral immune exhaustion, suggesting that targeting both immune checkpoints could be a promising therapeutic strategy. Despite low PD-L1

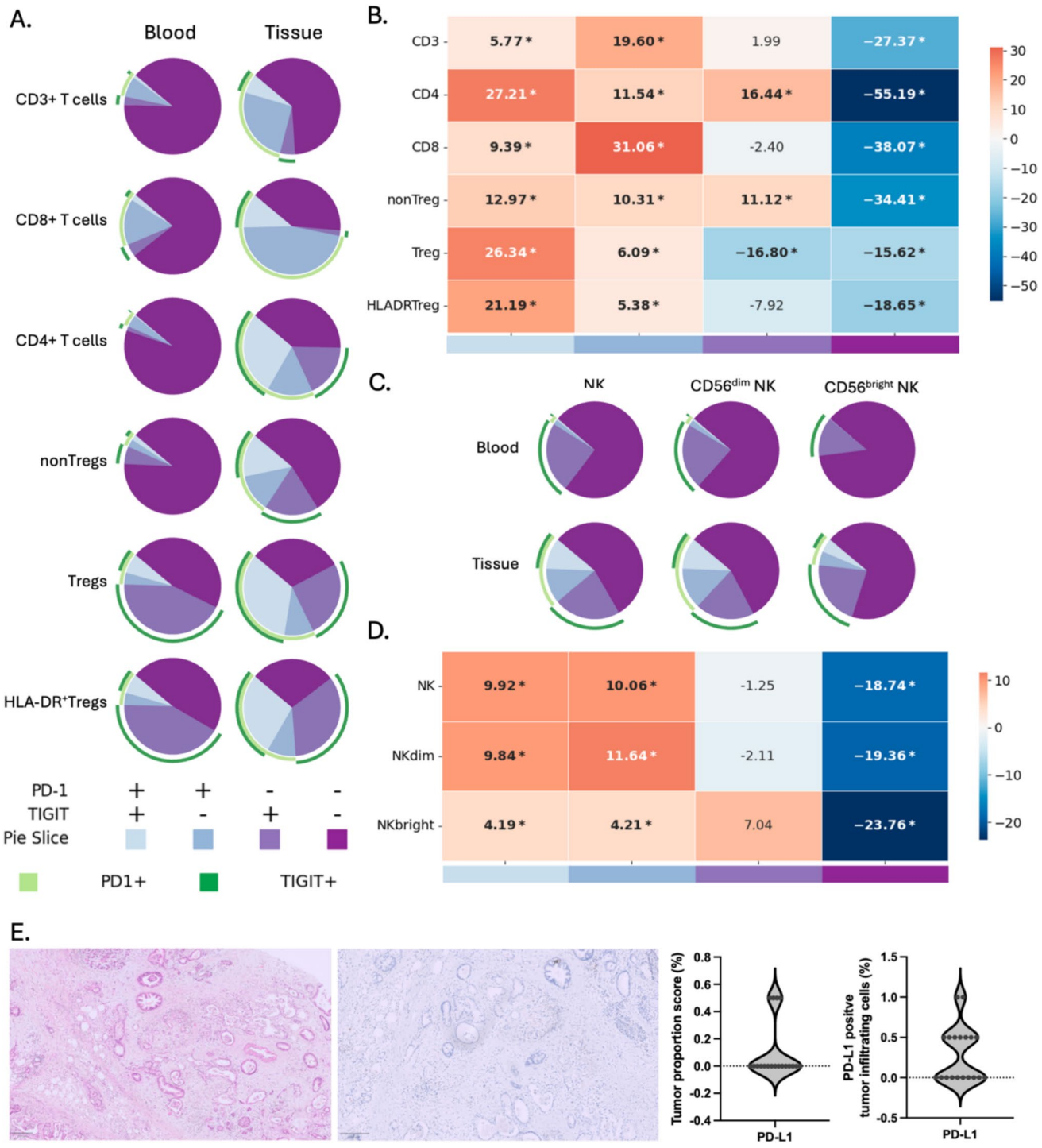
A.
Blood
Tissue
CD3+ T cells
CD8+ T cells
CD4+ T cells
nonTregs
Tregs
HLA-DR+Tregs
PD-1 + + - -
TIGIT + - + -
Pie Slice
PD1+
TIGIT+
B.
CD3 5.77* 19.60* 1.99 −27.37*
CD4 27.21* 11.54* 16.44* −55.19*
CD8 9.39* 31.06* -2.40 −38.07*
nonTreg 12.97* 10.31* 11.12* −34.41*
Treg 26.34* 6.09* −16.80* −15.62*
HLADRTreg 21.19* 5.38* -7.92 −18.65*
30 20 10 0 −10 −20 −30 −40 −50
C.
NK
CD56dim NK
CD56bright NK
Blood
Tissue
D.
NK 9.92* 10.06* -1.25 −18.74*
NKdim 9.84* 11.64* -2.11 −19.36*
NKbright 4.19* 4.21* 7.04 −23.76*
10 0 −10 −20
E.
Tumor proportion score (%)
0.8 0.6 0.4 0.2 0.0 -0.2 -0.4
PD-L1
PD-L1 positve tumor infiltrating cells (%)
1.5 1.0 0.5 0.0 -0.5
PD-L1

◂**Fig. 5** Co-targeting TIGIT and PD-1 may offer valuable therapeutic potential in PDAC **A** Pie charts depicting the proportion of T cell subsets expressing PD-1 and/or TIGIT in peripheral blood (left column) and tumor tissue (right column). Arcs are color-coded to indicate expression categories: PD-1$^+$ (light green arcs), TIGIT$^+$ (dark green arcs), and co-expression as defined in the legend. **B** Heatmap showing the absolute difference in the proportion of T cell subpopulations co-expressing of PD-1 and/or TIGIT between peripheral blood and tumor tissue. The color scale represents changes in percentage, with decrease (blue) and increase (red) in the tumor. Statistical significance was determined using a linear mixed-effect model with Benjamini–Hochberg correction; p-values < 0.05 were considered significant and marked in bold with an *. **C** Pie charts illustrating the proportion of NK cell subsets expressing PD-1 and/or TIGIT in peripheral blood (upper row) and tissue (lower row). Color coding follows the same scheme as in panel (A). **D** Heatmap showing the absolute difference in percentage positive NK cell subpopulations co-expressing of PD-1 and/or TIGIT. The color scale represents changes in percentage, with decrease (blue) and increase (red) in the tumor. Statistical significance was determined using a linear mixed-effect model with Benjamini–Hochberg correction; p-values < 0.05 were considered significant and marked in bold with an *. **E** Representative immunohistochemistry images showing hematoxylin–eosin staining and PD-L1 staining. Right panel shows violin plots quantifying PD-L1 expression, represented as the tumor proportion score (percentage of PD-L1-positive tumor cells) and the percentage of PD-L1-positive infiltrating immune cells across all patients

expression in PDAC, combined targeting of PD-1 and TIGIT may offer improved clinical outcomes. These findings support clinical investigation of dual checkpoint inhibition as a treatment strategy for PDAC.

Supplementary Information The online version contains supplementary material available at https://doi.org/10.1007/s00262-026-04343-w.

Acknowledgements The authors wish to acknowledge the support of the Antwerp Biobank for providing the patient samples that were used in this study.

Author contributions DQ and JVA conceptualized and designed the study. DQ performed the majority of the experimental work. CH and HL carried out the immunohistochemistry experiments, and DP scored the stainings. KZ assisted with performing the PD-L1 IHC staining and scanning the slides. GR collected patient samples and coordinated patient recruitment, surgery, and clinical metadata collection. JC and CF helped with the statistical analyses. DQ conducted most of the data analysis, with input from JVA, JDW, JC and CF. Data interpretation was carried out by DQ with assistance of JVA, JDW, and ES. DQ wrote the original draft of the manuscript. All authors (YV, SVdH, DP, JC, CH, HL, KZ, PVD, MP, HP, SK, JDW, CF, FL, GR, ES, JVA) contributed to reviewing and editing the manuscript. Supervision was provided by ES, JVA, and GR. Funding was acquired by DQ, FL, ES, and JVA. All authors read and approved the final manuscript.

Funding This research project has been funded by UAntwerp (FFB190245 and PP230000). D.Q. and Y.V. were PhD fellows of the Research Foundation Flanders (FWO; grants 1S76421N and 1S69721N). This work was also supported by a Belgian Week of Gastroenterology (BWGE) grant. We would like to thank several patrons, as part of this research was funded by donations from different donors, including Dedert Schilde vzw, Willy Floren, and the Vereycken family.

Data availability The datasets generated during the current study are not publicly available due to patient privacy but are available from the corresponding author upon reasonable request.

Declarations

Conflict of interest The authors declare no conflict of interest.

Consent to participate Informed consent was obtained from all individual participants included in the study.

Ethical approval
This study was approved by the Ethics Committee of the University of Antwerp (Antwerp, Belgium) and the Antwerp University Hospital (Antwerp, Belgium) under the reference number 14/47/480.

References

1. Siegel RL, Giaquinto AN, Jemal A (2024) Cancer statistics, 2024. CA Cancer J Clin 74:12–49
2. Jain A, Bhardwaj V (2021) Therapeutic resistance in pancreatic ductal adenocarcinoma: current challenges and future opportunities. World J Gastroenterol 27:6527
3. Neoptolemos JP et al (2004) A randomized trial of chemoradiotherapy and chemotherapy after resection of pancreatic cancer. N Engl J Med 350:1200–1210
4. Oettle H et al (2013) Adjuvant chemotherapy with gemcitabine and long-term outcomes among patients with resected pancreatic cancer: the CONKO-001 randomized trial. JAMA 310:1473–1481
5. Neoptolemos JP et al (2010) Adjuvant chemotherapy with fluorouracil plus folinic acid versus gemcitabine following pancreatic cancer resection a randomized controlled trial. JAMA 304(10):1073–1081
6. Conroy T et al (2022) Five-year outcomes of FOLFIRINOX versus gemcitabine as adjuvant therapy for pancreatic cancer: a randomized clinical trial. JAMA Oncol 8:1571–1578
7. Sohal DPS et al (2016) Metastatic pancreatic cancer: American society of clinical oncology clinical practice guideline. J Clin Oncol 34:2784–2796
8. Shiravand Y et al (2022) Immune checkpoint inhibitors in cancer therapy. Curr Oncol 29:3044

9. Brahmer JR et al (2012) Safety and activity of anti-PD-L1 antibody in patients with advanced cancer. N Engl J Med 366:2455
10. Royal RE et al (2010) Phase 2 trial of single agent ipilimumab (anti-CTLA-4) for locally advanced or metastatic pancreatic adenocarcinoma. J Immunother 33:828
11. Patnaik A et al (2015) Phase I study of pembrolizumab (MK-3475; anti-PD-1 monoclonal antibody) in patients with advanced solid tumors. Clin Cancer Res 21:4286–4293
12. O'Reilly EM et al (2019) Durvalumab with or without tremelimumab for patients with metastatic pancreatic ductal adenocarcinoma: a phase 2 randomized clinical trial. JAMA Oncol 5:1431
13. Capurso G, Sette C (2019) Drug resistance in pancreatic cancer: new player caught in act. EBioMedicine 40:39–40
14. Hsu SK et al (2022) Culprits of PDAC resistance to gemcitabine and immune checkpoint inhibitor: tumour microenvironment components. Front Mol Biosci 9:1020888
15. Steele NG et al (2020) Multimodal mapping of the tumor and peripheral blood immune landscape in human pancreatic cancer. Nat Cancer 1:1097
16. Freed-Pastor WA et al (2021) The CD155/TIGIT axis promotes and maintains immune evasion in neoantigen-expressing pancreatic cancer. Cancer Cell 39:1342-1360.e14
17. Sivakumar S et al (2025) (2025) Distinct immune cell infiltration patterns in pancreatic ductal adenocarcinoma (PDAC) exhibit divergent immune cell selection and immunosuppressive mechanisms. Nat Commun 16(1):1–20
18. Harjunpää H, Guillerey C (2019) TIGIT as an emerging immune checkpoint. Clinical Exp Immunol. https://doi.org/10.1111/cei.13407
19. Shibuya A, Shibuya K (2021) DNAM-1 versus TIGIT: competitive roles in tumor immunity and inflammatory responses. Int Immunol 33:687–692
20. Banta KL et al (2022) Mechanistic convergence of the TIGIT and PD-1 inhibitory pathways necessitates co-blockade to optimize anti-tumor $CD8^+$ T cell responses. Immunity 55:512
21. Cho BC et al (2022) Tiragolumab plus atezolizumab versus placebo plus atezolizumab as a first-line treatment for PD-L1-selected non-small-cell lung cancer (CITYSCAPE): primary and follow-up analyses of a randomised, double-blind, phase 2 study. Lancet Oncol 23:781–792
22. Johnston RJ et al (2014) The Immunoreceptor TIGIT regulates antitumor and antiviral $CD8^+$ T cell effector function. Cancer Cell 26:923–937
23. Yamamoto N et al (2024) Phase I study of the anti-TIGIT antibody tiragolumab in combination with atezolizumab in Japanese patients with advanced or metastatic solid tumors. Cancer Chemother Pharmacol 94:109–115
24. Tang Z, Kang B, Li C, Chen T, Zhang Z (2019) GEPIA2: an enhanced web server for large-scale expression profiling and interactive analysis. Nucleic Acids Res 47:W556
25. Brierley JD, Gospodarowicz MK, Wittekind C (2017) TNM classification of malignant tumours - Google Books. Wiley, London
26. Joller N et al (2014) Treg cells expressing the coinhibitory molecule TIGIT selectively inhibit proinflammatory Th1 and Th17 cell responses. Immunity 40:569–581
27. Ju Y et al (2024) Barriers and opportunities in pancreatic cancer immunotherapy. NPJ Precis Oncol 8(1):1–18
28. Kabacaoglu D, Ciecielski KJ, Ruess DA, Algül H (2018) Immune checkpoint inhibition for pancreatic ductal adenocarcinoma: current limitations and future options. Front Immunol 9:396649
29. Chiang EY, Mellman I (2022) TIGIT-CD226-PVR axis: advancing immune checkpoint blockade for cancer immunotherapy. J Immunother Cancer. https://doi.org/10.1136/jitc-2022-004711
30. Liew SZH et al (2023) Geographical, ethnic, and genetic differences in pancreatic cancer predisposition. Chin Clin Oncol 12:27–27
31. Park W, Chawla A, O'Reilly EM (2021) Pancreatic cancer: a review. JAMA 326:851
32. Ni B et al (2023) (2023) Crosstalk between peripheral innervation and pancreatic ductal adenocarcinoma. Neurosci Bull 39(11):1717–1731
33. Goess R et al (2024) Lymph node examination and survival in resected pancreatic ductal adenocarcinoma: retrospective study. BJS Open 8(1):zard125
34. Carstens JL et al (2017) (2017) Spatial computation of intratumoral T cells correlates with survival of patients with pancreatic cancer. Nat Commun 8(1):1–13
35. Blando J et al (2019) Comparison of immune infiltrates in melanoma and pancreatic cancer highlights VISTA as a potential target in pancreatic cancer. Proc Natl Acad Sci USA 116:1692–1697
36. Tang Y et al (2014) An increased abundance of tumor-infiltrating regulatory T cells is correlated with the progression and prognosis of pancreatic ductal adenocarcinoma. PLoS ONE 9:e91551
37. Jacquelot N et al (2017) Predictors of responses to immune checkpoint blockade in advanced melanoma. Nat Commun 8(1):1–13
38. Kumagai S et al (2020) The PD-1 expression balance between effector and regulatory T cells predicts the clinical efficacy of PD-1 blockade therapies. Nat Immunol 21:1346–1358
39. Ma X et al (2023) Human HLA-DR+CD27+ regulatory T cells show enhanced antigen-specific suppressive function. JCI Insight. https://doi.org/10.1172/jci.insight.162978
40. Baecher-Allan C, Wolf E, Hafler DA (2006) MHC class II expression identifies functionally distinct human regulatory T cells. J Immunol 176:4622–4631
41. Lim SA et al (2019) Defective localization with impaired tumor cytotoxicity contributes to the immune escape of NK cells in pancreatic cancer patients. Front Immunol 10:496
42. Persky J et al (2024) Characterization of natural killer and cytotoxic T-cell immune infiltrates in pancreatic ductal adenocarcinoma. J Surg Oncol 129:885–892
43. Stannard KA et al (2019) Human peripheral blood DNAM-1neg NK cells are a terminally differentiated subset with limited effector functions. Blood Adv 3:1681
44. Reymond N et al (2004) DNAM-1 and PVR regulate monocyte migration through endothelial junctions. J Exp Med 199:1331
45. Bottino C et al (2003) Identification of PVR (CD155) and Nectin-2 (CD112) as cell surface ligands for the human DNAM-1 (CD226) activating molecule. J Exp Med 198:557
46. Chan CJ et al (2010) DNAM-1/CD155 interactions promote cytokine and NK cell-mediated suppression of poorly immunogenic melanoma metastases. J Immunol 184:902–911
47. Sanchez-Correa B et al (2012) Decreased expression of DNAM-1 on NK cells from acute myeloid leukemia patients. Immunol Cell Biol 90:109–115
48. Saunders PM et al (2025) CD155 density on target cells drives divergent natural killer cell responses owing to DNAM-1 loss. J Immunol. https://doi.org/10.1093/JIMMUN/VKAF293
49. Fourcade J et al (2018) CD226 opposes TIGIT to disrupt tregs in melanoma. JCI Insight. https://doi.org/10.1172/jci.insight.121157
50. Brown ME et al (2022) Human CD4+CD25+CD226-tregs demonstrate increased purity, lineage stability, and suppressive capacity versus CD4+CD25+CD127lo/-tregs for adoptive cell therapy. Front Immunol 13:873560
51. Ma J et al (2023) CD226 maintains regulatory T cell phenotype stability and metabolism by the mTOR/Myc pathway under inflammatory conditions. Cell Rep 42:113306
52. Chauvin JM, Zarour HM (2020) TIGIT in cancer immunotherapy. J ImmunoTher Cancer. https://doi.org/10.1136/jitc-2020-000957

53. Heiduk M et al (2023) TIGIT expression delineates T-cell populations with distinct functional and prognostic impact in pancreatic cancer. Clin Cancer Res 29:2638–2650
54. Liang S et al (2015) The clinical and pathological significance of Nectin-2 and DDX3 expression in pancreatic ductal adenocarcinomas. Dis Markers 2015:379568
55. Nishiwada S et al (2015) Clinical significance of CD155 expression in human pancreatic cancer. Anticancer Res 35:2287–2297
56. Agorku DJ, Bosio A, Alves F, Ströbel P, Hardt O (2024) Colorectal cancer-associated fibroblasts inhibit effector T cells via NECTIN2 signaling. Cancer Lett 595:216985
57. Yin Y et al (2023) High density and proximity of $CD8^+$ T cells to tumor cells are correlated with better response to nivolumab treatment in metastatic pleural mesothelioma. Thorac Cancer 14:1991–2000